CRYSTAL GROWTH & DESIGN

Subscriber access provided by UNIV OF WESTERN ONTARIO

Article

Zn2GeO4/SnO2 nanowire heterostructures driven by Plateau-Rayleigh instability

Jaime Dolado, Kate L Renforth, James E Nunn, Steven A Hindmarsh, Pedro Hidalgo, Ana M. Sanchez, and Bianchi Mendez

Cryst. Growth Des., **Just Accepted Manuscript** • DOI: 10.1021/acs.cgd.9b01494 • Publication Date (Web): 15 Nov 2019

Zn_2GeO_4/SnO_2 nanowire heterostructures driven by Plateau-Rayleigh instability

Jaime Dolado,[†] Kate L Renforth,[‡] James E Nunn,[‡] Steve A. Hindsmarsh,[‡] Pedro Hidalgo,[†] Ana M Sánchez,[*,‡] and Bianchi Méndez[*,†]

[†]*Department of Materials Physics, Faculty of Physical Sciences, University Complutense of Madrid, E-28040 Madrid, Spain*

[‡]*Department of Physics, University of Warwick, Coventry, CV4 7AL, United Kingdom*

E-mail: a.m.sanchez@warwick.co.uk; bianchi@ucm.es

Abstract

Herein, we report the formation of a particular core-shell structure, with a zinc germanate (Zn_2GeO_4) nanowire core and a discontinuous shell of SnO_2 nanocrystals, obtained in a single step process. We propose a growth model that combines the Plateau-Rayleigh mechanism to produce a pattern of amorphous germanium oxide (a-GeO_2) particles along the Zn_2GeO_4 nanowire, and the subsequent growth of well-faceted SnO_2 crystals when the nanowire orientation meets good lattice matching conditions. In this latter case, the linear array of a-GeO_2 particles acts as nucleation sites for the SnO_2 crystallites leading to a skewer-like morphology that retains the periodicity of the Plateau-Rayleigh process. Otherwise, nanowires with different orientations appear decorated with a pattern of a-GeO_2 beads mimicking a necklace. Atomic resolution electron microscopy has been used to characterize the Zn_2GeO_4/SnO_2 nanoheterostructures. Besides, optical confinement effects have been observed in the luminescence maps and spectra, which have potential for further exploitation in the design of optical microcavities.

Introduction

The synthesis and design of low-dimensional nanostructures based on semiconductor oxides give access to materials systems with novel properties that otherwise would not be possible. In particular, nanowires (NWs) can act as support for other nanomaterials, such as nanoparticles, other nanowires or nanosheets, leading to architectures not available (or difficult to achieve) through conventional thin film technology. Chemical Vapor Deposition (CVD) or Molecular Beam Epitaxy (MBE) are commonly used to grow high quality nanomaterials in a controlled manner. However, most of the effort have been devoted to III-V semiconductors. Examples of mixed dimensionality involving III-V NWs have been already reported in the literature, such self-assembled quantum dots embedded in NWs for light emitting devices.[1–3]

Architectures based on NWs with different physical properties are also raising scientific interest, such as hybrid superconductor-III-V semiconductor nanowire junctions that were explored as quantum transport devices.[4] Alternatively, wide band gap (WBG) oxides, such as Zn_2GeO_4 or Ga_2O_3, are emerging as effective competitors to traditional WBG semiconductors, i.e. III-nitride, for high power and ultraviolet optoelectronic applications.[5,6] Semiconductor oxides NWs provided an excellent technological platform based on the synergy between the physical properties of oxides and the 1D morphology of the NWs. One of the main challenges in oxide nanomaterials is the reproducibility of nanostructures with a chosen morphology and physical properties. Unfortunately, the fabrication of these structures is not always straightforward and have been less investigated in comparison with III-V semiconductor technology. Self-assembly mechanisms usually provide the required reproducibility of the nanostructures and facilitate the fabrication process via a bottom-up strategy.[7] Growth based on thermal evaporation methods constitutes an effective way to obtain a huge variety of oxide nanowires by tuning the growth parameters, such as temperature, duration, precursors and gas flow. Generally, minimization of surface energy favors anisotropic growth and nanowires with preferred orientations are produced.[8] In addition, dopant out-diffusion in nanowires may modify the properties of the NW surfaces, favoring the eventual formation

of complex nanostructures in a one-step process. We have previously reported the role of Sn and Cr impurities in the shape engineering of complex SnO_2/Ga_2O_3 nanowires.[9] In that case, the orientation and doping of the central Ga_2O_3 nanowire determined the formation of SnO_2 crystals or SnO_2 crossing wires. Thus, the NW surface has a critical role in the production of more complex nanostructures. Recently, the Plateau-Rayleigh (P-R) instability, which describes e.g. the splitting of a column of water into droplets to minimize surface tension, has been invoked to explain the growth mechanism of a diameter-modulated shell around Si and Ge NWs.[10] In this mechanism the NW thicknesses and diffusion coefficients of the chemical species are key factors in the spontaneous formation of a droplet pattern along the NW. In this work, we report the structure and optical properties of an array of SnO_2 particles evenly distributed along Zn_2GeO_4 nanowires, which have been produced by the combination of the P-R crystal growth and vapor-solid mechanisms in a single-step process.

We focus on oxide architectures based on zinc germanate (Zn_2GeO_4), a promising transparent conductive oxide with a wide bandgap of 4.7 eV with quite acceptable electronic conductivity.[11–13] This ternary oxide has emerged as an attractive oxide among wide band gap materials for optoelectronic applications, such as phosphors[14] or solar blind photodetectors.[15] In particular, Zn_2GeO_4 nanowires have also been probed as efficient injection material in electroluminescence devices.[16] Besides, its lattice structure is suitable to host small cations ions, such as Li, rendering promising applications in batteries.[17] Zn_2GeO_4 has a rhombohedral structure built up by corner-sharing GeO_4 and ZnO_4 tetrahedra, aligned parallel to the c-axis in a pattern of Zn + Zn + Ge + Zn + Zn + Ge + ... The crystal belongs to the space group $R\bar{3}$ with lattice parameters, in the hexagonal setting, of $a = 14.23$ Åand $c = 9.53$ Å.[18] We have already reported the formation of single Zn_2GeO_4 rods, a few microns long, via thermal treatment of a mixture of zinc oxide, germanium and graphite.[19] The presence of Zn and Ge cations in the oxide could lead to novel features not feasible in binary oxides. In this work, we explore the formation of oxide complex heterostructures based on Zn_2GeO_4 nanowires by adding tin oxide into the precursors. Thus, Zn_2GeO_4 NWs/SnO_2

heterostructures are formed in a single step process, with the P-R mechanism playing a key role. The morphology, microstructure and composition of these nano-heterostructures have been carried out by electron microscopy and associated techniques. A growth model is postulated based on the information obtained from the structural analysis. The optical properties of these functional materials have been revealed using cathodoluminescence and photoluminescence. Currently, it is easy to envisage the potential of these heterostructures in optoelectronic applications, since the size and shape of the obtained nanostructures may sustain optical modes in the visible range with a well-defined arrangement along a central NW.

Experimental

The synthesis of the NW heterostructures were carried out by a thermal evaporation method. The material precursors were a compacted mixture of ZnO:Ge:C powders (2:1:2 wt.%)), where SnO_2 powders were added in proportions of 5, 10 and 15 wt.% related to the total ZnO:Ge amount. These precursors acted as source and substrate, with no foreign catalyst. The thermal treatments were conducted at 800 °C for 8 hours under an Ar flow of 1.5 l/min. The structure and morphology of the obtained products were analyzed by Scanning Electron Microscopy (SEM) in a Hitachi S-2500 equipped with cathodoluminescence (CL) setup, and high resolution (Scanning) Transmission Electron Microscopy ((S)TEM) using a JEOL 2100 and a double corrected ARM 200F microscopes working at 200 kV. The cross-sectional samples were obtained by means of a JEOL 4500 Focused Ion Beam (FIB)/SEM with a 30 kV ion column and a Ga^+ ion source. Energy dispersive X-ray spectroscopy (EDX) analyses were performed with probe currents of approximately 200 pA and collected with an Oxford Instruments X-Max Silicon Drift Detector with an area of 100 mm_2. The optical characterization was completed with the aid of a confocal optical microscope Horiba-Jobin-Ybon LabRam HR800 using a 325 nm laser as excitation source.

Results and discussion

It has previously been found that the presence of Sn at impurity level can modify the production yield of some oxides nanostructures, including Ga_2O_3 or GeO_2.[20,21] Here, SnO_2 powders have been added to the precursor mixture in proportions of 5, 10 and 15 wt.% related to the total ZnO:Ge amount and the same thermal treatment was conducted for all the samples. Samples were labelled as: T-x, where x is % of SnO_2 added to the precursor mixture. T-x pellets act simultaneously as source and substrate with no other foreign catalyst. After the thermal treatment, the nanostructures formed on the pellets were transferred onto silicon substrates and/or TEM grids to be analyzed.

The morphology of the nanostructures grown from the different pellets were first analyzed using scanning electron microscopy (SEM) and results can be found in the Suppl. Inf. Figures S1 (a)-(c) show representative SEM images of the Zn_2GeO_4 nanostructures obtained from T-5, T-10 and T-15, respectively, revealing some distinctive features as the concentration of Sn increases. Ultra-long and thin Zn_2GeO_4 nanowires with diameters of 100 – 300 nm and up to a hundred microns in length were obtained in the T-5 pellet (lowest Sn concentration). Some Zn_2GeO_4 NWs are decorated with small *beads* forming a long necklace-like (NL) structure (Figure 1(a)). When using T-10 substrate, skewer-like (SK) morphologies were formed (Figure 1(c)) in addition to the Zn_2GeO_4 NWs and NLs. They consist of a straight central wire with surrounding well-faceted particles. The size and frequency of the particles vary between structures, though their diameter (typically 1-2 μm) is often several times larger than that of the wire (100 – 300 nm). This SK-like structure has been also observed before for Ga_2O_3 nanowires with SnO_2 particles obtained by thermal evaporation methods.[9] Finally, thermal treatment of T-15 pellets leads to the formation of all nanostructure types: single nanowires, necklaces and skewers. The elemental composition of the nanostructures was evaluated using energy-dispersive X-ray spectroscopy (EDS) and the results are displayed in Figures 1(b) and 1(d). In both NLs and SKs the EDS maps demonstrate that the central wire is composed of Zn_2GeO_4, determined by the 2:1 ratio

of Zn:Ge in the X-ray microanalysis spectra (not shown). Regarding the NL, the smooth appearance of the beads in NLs suggests an amorphous germanium oxide (a-GeO_2) particle, (confirmed below by TEM analysis), with no Zn or Sn. The faceted particles in the SKs are mainly composed of Sn and O, i.e. tin oxide particles. Here again, no Zn was observed in the attached particles in the SK structure, but the presence of non-negligible amount of Ge was detected. Ge was detected in the majority of SnO_2 particles, both in T-10 and T-15 growths, with a variable Ge/Sn proportion ranging from 8-17 at.%. These results demonstrate that a low Sn content (T-5) in the substrate produces just Zn_2GeO_4 NWs and eventually the appearance of a-GeO_2 droplets periodically distributed along the sidewalls of the nanowires. By increasing the amount of Sn in the precursors, additional SnO_2 particles are formed on certain Zn_2GeO_4 NWs leading to Zn_2GeO_4/SnO_2 heterostructures.

The crystal structure of the NL and SK systems was determined by high-resolution transmission electron microscopy (HRTEM). We analyzed the crystal structure of the Zn_2GeO_4 NW axis in both the NL and SK structures. Figure 2(a) shows a low-magnification TEM image of a NL-structure. Figures 2(b) and (c) are a HRTEM image and a selected area electron diffraction (SAED) pattern respectively, recorded in the NW area of Figure 2(a). The SAED pattern and HRTEM image corresponds to the Zn_2GeO_4 rhombohedral structure viewed along a [1-10] zone axis, revealing the growth direction of the NW to be $\langle 110 \rangle$. HRTEM image in Figure 2(b) shows that the NW surface is coated by a thin (5-7 nm) amorphous layer. ADF-STEM images of a detail of the NW surface-amorphous bead interface are shown in the Figures 2(d) and (e).

The generation of amorphous oxide thin layer on a NW surfaces is often observed, especially if the growth process takes place at high temperatures in an unsealed furnace. In particular, the presence of germanium oxide around Zn_2GeO_4 obtained by thermal deposition methods have already been reported both in thin films and thermal treated ZnO:Ge mixtures. Thus, Zheng *et al.*.[22] demonstrated that GeO clusters can be found in Zn_2GeO_4 thin films by thermal annealing of Ge/ZnO multilayers. On the other hand, other observa-

tions indicated that when the amount of Ge exceeded the solid solubility limit of Ge in ZnO, the formation of the new compounds Zn_2GeO_4 and GeO results.[23] Uniform GeO_2-Zn_2GeO_4 chain-like nanostructures grown by a vapor phase reaction have been reported, in which a Ge vapor formed a GeO shell layer on the NWs.[24] Our results suggest a surface oxidation of Zn_2GeO_4 NWs due to Ge out-diffusion and air ingress during thermal treatment. The addition of Sn helps this process, since the Sn atoms substitute onto Ge sites, allowing Ge out-diffusion and the formation of a GeO_2 shell. We find that the same thermal treatment without any Sn in the precursor only produces Zn_2GeO_4 microrods with lateral dimensions of about 1 micron, without any GeO_2. Therefore, Sn impurities limit somehow the thickness of the wires by producing a kind of an amorphous wetting layer of germanium oxide (a-GeO_2) that prevent the lateral growth of the Zn_2GeO_4 wires. However, we have also observed that some total or partial dewetting of this a-GeO_2 shell may occur, leading to the formation of an array of beads along the Zn_2GeO_4 NWs. The occurrence of periodic droplets around nanowires has been previously reported in various materials, such as Si/Ge, Ge/Ge, GaP/GaO_x or SiC/SiO_2 systems, claiming the P-R instability as the main formation mechanism.[25–27] This mechanism is based on the total surface energy reduction and it is controlled by the atom diffusion lengths.[28] Day *et al.*[25] proposed the P-R instability phenomenon as the driving force to form a periodic array of Ge particles instead of a conformal shell around Si or Ge NWs. Later on, the P-R mechanism was also invoked as the formation mechanism of SiC/SiO_2 nanochains composed by a crystalline SiC core, an amorphous SiO_2 shell and a periodic array of SiO_2 beads[29] and in GaP/GaO_x core-shell NWs[30] , via vapor solid deposition methods at higher temperatures. Under these conditions, the saturated vapor pressure and viscosity of intermediate products could also play a role since the process takes place at temperatures closer to the melting point. The P-R instability is described as the constant-volume transformation of 1D liquids and solids that reduce the total tension or surface energy. Thus, size effects are relevant for the process, such as the thickness of the layer and the diameter of the nanowire.[28] In the case of thin layers around NWs, the models

predict a linear relationship between the diameter of the NW and the spacing between the produced particles.[31] Figure 1(e) plots the length separation period between beads versus the NW diameter for several NLs obtained in this work. The linear dependence found is a signature of the P-R mechanism. In addition, the growth temperature, close to the melting point of precursors, favors atomic diffusion along the NW surface. Therefore, the thermodynamic and kinetic conditions promote the formation of evenly *a*-GeO_2 droplets along the NW in a P-R scheme.

SK architectures are also developed in the pellet when Sn amount increases. Figure 3(a) corresponds to a low magnification TEM image of the SK nanostructures, with the red and yellow circles indicating the areas of Zn_2GeO_4 NW and SnO_2 particle, respectively, where the SAED patterns were recorded (Figure 3(b) and (c)). The SAED pattern enables the identification of the rhombohedral and rutile structures for the Zn_2GeO_4 NW and SnO_2 particle, respectively. Additionally, we determined that the Zn_2GeO_4 NW grows along the [001] direction and the SnO_2 particles exhibit {110} facets truncated by (002) planes when viewed along $[1\bar{1}0]$. The high-resolution TEM images of the NW and particle (Figure S2) corroborate those results. Zn_2GeO_4 NW image reveal (110) and (003) planes (d = 0.714 nm and 0.3182 nm, respectively). From Figure S2 it is inferred that SnO_2 (110) planes are parallel to the Zn_2GeO_4 NW. Good lattice matching is present between these planes, since cation distances for (110) Zn_2GeO_4 and (110) SnO_2 planes are 3.178 and 3.187 Å, respectively. Further characterization of the SK structures, cross-section specimens, parallel and perpendicular to the nanowire were prepared using Focused Ion Beam (FIB). Figures 3(d)-(e) correspond the ADF-STEM and EDS maps results from the FIB samples prepared by cutting parallel to the NW long axis. The high-resolution ADF images from the central NW and FFT analysis confirm the [001] growth direction of the Zn_2GeO_4 NW (shown in Figure S3). The microanalysis results of the particles yield SnO_2 heavily doped with Ge (Figure 3(e)). The Ge map shows that some Ge segregation takes place leaving higher Ge concentration at the lateral surfaces of the particles. The Sn/Ge ratio detected is too high to

consider Ge just a dopant impurity. Table S1 shows the Sn and Ge elemental composition for a range of particles (O content has been omitted since quantitative EDX of light elements is often unreliable). The Ge atomic proportion varies from 8% to 17%. Such values suggest the formation of a ternary oxide, i.e. a $Sn_{1-x}Ge_xO_2$-type solid solution that retains the rutile structure.[32] However, the solid solubility of GeO_2 in SnO_2 has been found to be limited to 6% after calcination of constituent oxides at 1100 °C,[33] which is much less than our measurement. The ionic radius of Ge^{4+} (0.053 nm) is considerably smaller than that of Sn^{4+} (0.069 nm). Therefore, the presence of Ge in the SnO_2 rutile structure implies some strain in the particles, since Ge^{4+} is expected to replace Sn^{4+} sites, although the differences in the measured values from SAED of particles and theoretical rutile structure are too small to be determined reliably.

To further analyse the Zn_2GeO_4/SnO_2 heterojunction a FIB specimen section perpendicular to the NW was prepared from a T-15 growth. Figure 4(a) corresponds to a low magnification ADF image of this section where the hexagonal Zn_2GeO_4 nanowire core is clearly revealed. Figure 4(b) displays the atomic resolution ADF-STEM image of the NW/particle interface. These measurements show that SnO_2 lattice must insert a central Zn_2GeO_4 nanowire that expose facets with $(\bar{2}10)$ $(\bar{1}20)$ and (110) planes, in agreement with its [001] orientation. It can also be seen that at the interface there is good alignment of (020) planes in SnO_2 and (330) planes in Zn_2GeO_4, displayed as a set of black and white lines, respectively. (200) planes for the SnO_2 particle and $(3\bar{6}0)$ planes for the Zn_2GeO_4 wire have been marked at the interface in Figure 4(c). These planes have a very similar inter-planar spacing. Although they are not perfectly aligned, they are close enough to provide a good epitaxial lattice matching at the interface. It has been noted that for radial heterostructures such as this NW-particle, a significantly larger lattice mismatch strain can be elastically accommodated than traditional planar structures,[34] with theoretical predictions that such structures could allow 5-10 times more strain than planar structures.

Based on the TEM/STEM imaging and EDS elemental analysis presented in Figures

2 to 4, the following growth model for NL and SK nano-heterostructures is proposed and sketched in Figure 3(f). Thermal growth of the precursors lead to the formation of Zn_2GeO_4 nanowires, and for many of them an array of a-GeO_2 beads along the central Zn_2GeO_4 NW is produced via the P-R mechanism, as described above. This is the trend in samples produced in growth T-5. Then, the a-GeO_2 beads would act as preferential sites for the nucleation of tin oxide crystallites in the Zn_2GeO_4 NWs when Sn concentration increases (T-10 and T-15). This could explain the rather high Ge content detected in the SnO_2 crystals and the similar pattern of crystallites along the central wire. TEM measurements have shown that Zn_2GeO_4 NWs grow along [110] and [001] directions. The fact that not all the necklaces have become skewers could be related to the particular orientation of the central Zn_2GeO_4 NW, with different sidewall planes. In particular, Zn_2GeO_4 NW along the [001] orientation favors the nucleation of tin oxide crystallites, as discussed above. On the other hand, the amorphous nature of the germanium oxide beads in NLs should not demand a preferred orientation of the central Zn_2GeO_4 NW. The lateral size of the SnO_2 crystals formed on [001] NWs can reach up to 1-2 microns in diameter as maximum size, however their growth can continue parallel to the NW sidewalls, leading in some cases to a quasi-fully coated NW in a core-shell morphology. This is consistent with the fact that {110} are the lower surface energy planes in SnO_2.

The particular nature of the NL and SK structures may influence their physical properties. Semiconducting oxides usually contain a high number of native defects, such as oxygen vacancies and cations interstitials. These defects introduce electronic levels in the band gap and hence affect dramatically the optical and electronic properties of the semiconductor oxides. An easy way to test electronic states is by luminescence techniques that skip electrical contact issues, which can be a serious experimental drawback, especially when it comes to nanowires. In order to assess the optical properties of the NL and SK structures and to find eventual applications, we have carried out monochromatic cathodoluminescence (CL) imaging and spectra in the SEM, which has the advantage of high spatial resolution,

and photoluminescence (PL) measurements in a confocal optical microscope. Luminescence studies of Zn_2GeO_4 are scarce and the luminescence mechanisms are still not clear. Its band gap is around 4.7 eV, hence near band edge luminescence is not observed straightforwardly. The reported luminescence bands of Zn_2GeO_4 are found to be dependent on the particular method used to prepare the material and the excitation conditions. In general, they have been assigned to defect related states that could involve Zn_i and oxygen vacancies.[35] In particular, undoped Zn_2GeO_4 microwires obtained by thermal methods show complex green (about 2.2 eV) and UV (3.3 eV) luminescence bands.[19,36,37] Figure 5(a) shows the CL image of a NL structure, where a remarkable increase of the CL intensity at the *a*-GeO_2 beads is noticed. Locally CL spectra recorded at the NW and at the bead are essentially the same and correspond to the UV Zn_2GeO_4 emission (Figure 5(d)), which indicates that no new bands arise from the amorphous beads. This band has been already reported by CL measurements in undoped Zn_2GeO_4 microrods.[19] It seems that the *a*-GeO_2 beads act as scattering centers and the luminescence escapes easily at these locations in comparison with uncoated NWs. In addition, some coupling effects seem to happen between adjacent beads at suitable beads separations, as it is shown in Figure 5(b). In some cases (Figure 5(b) top), light is confined between two beads leading to a nanowire segment brighter than the rest of the NW, while local quenching of the emission at a particular bead is also observed (Figure 5(b) bottom). This behaviour could be due to destructive and constructive interference of optical modes confined in the nanowire. Hence, the periodic arrangement of beads along the nanowire affects their luminescence properties. This requires further analysis.

Figure 5(c) shows the SEM and monochromatic CL images from a SK structure. CL spectra recorded in areas corresponding to the NW and at the particle are displayed in Figure 5(d). The CL spectrum from the NW axis (red line) displays a main emission band centered at around 3.3 eV. However, the CL spectrum at the particles (blue line) show two broad bands, which would be expected from the SnO_2 particles along with some luminescence from the central core. Luminescence from undoped SnO_2 is quite complex and the origin of

reported orange, green and blue emission bands, centred at 1.98 eV, 2.25 eV and 2.58 eV respectively, has been subject of discussion for many years.[38] Besides, in the case of crystals with small dimensions the role of the surface is relevant to the luminescence properties, since electronic states of defects are coupled to surface states.[39] In this work, we detect green-orange components at 2.05 eV and 2.30 eV, what means a slight displacement in comparison with other works.[40] The high Ge concentration measured by EDS would induce this slight modification in the defects-related band.

Finally, luminescence features in SK structures show their promising applications as optical microcavities. The size (in the range of hundred nanometers) and the well-faceted shape of the SnO_2 would allow for optical confinement, converting the crystals into optical microcavities. Light reflections between parallel facets of the crystallites would bring about Fabry-Perot resonances, or alternatively, reflections between adjacent facets in the crystal would lead to Whispering Gallery modes (WGM) resonances. Optical confinement in SnO_2 microtubes and ZnO-core/SnO_2 shell nanorods following different paths have been reported.[41,42] Here, we have observed optical resonances both in the CL and PL spectra of some SnO_2 crystals, as the ones showed in the PL spectrum of Figure 5(e). These resonances are originated from constructive interference of reflected light inside the crystallites. The Fabry-Perot resonance condition is $\lambda = 2nL_{FP}/N$, where L_{FP} is the cavity length, n the refractive index and N an integer. The separation of the wavelength maxima is related to the cavity length and the refractive index, which provide peaks separation according to the expression (Eq. 1):

$$\Delta\lambda = \frac{\lambda^2}{2L_{FP}(n - \lambda\frac{\mathrm{d}n}{\mathrm{d}\lambda})} \quad (1)$$

The refractive index has been estimated for each λ using the Cauchy formula, $n = A + B/\lambda^2$. The coefficients A and B and the cavity length, L_{FP}, have been obtained by fitting experimental PL maxima wavelengths with the above expressions (Figure 5(e)). The obtained values of the Cauchy coefficients, A = 1.9799 and B = 29210 nm^2 agree reasonably

with those reported for tin oxide.[43] On the other hand, the value of the optical pathway derived from the observed Fabry-Perot resonances, $L_{FP} = 3.83$ μm, matches with the length of the SnO_2 crystal (3.77 μm) measured in the SEM image of Figure 5(e). Optical resonances in shorter SnO_2 crystals (not shown) show higher $\Delta\lambda$, which supports these results. In spite of the rather poor quality of the optical resonances observed, we consider that the results are promising since they show that these Zn_2GeO_4 based nano-chains can be considered as a linear array of optical microcavities at different wavelengths, which cannot be easily built otherwise. Further work related to the incorporation of optical active ions will allow the wavelength tuning and possible optical interaction between the central NW and the periodic shell in oxide nanowires heterostructures.

Conclusions

In summary, nano-heterostructures based on Zn_2GeO_4 nanowires with evenly a-GeO_2 or SnO_2 crystalline particles around them have been obtained by a thermal evaporation method through a vapour-solid mechanism in a single step process. The growth conditions promote the formation of a periodic shell of a-GeO_2 particles, in a necklace configuration, around the Zn_2GeO_4 nanowires. The bead separation length scales linearly with the diameter of the NW, which supports the Plateau-Rayleigh instability as the formation mechanism. The driving force in the whole process is the lowering of the surface energy. Due to the lattice symmetries, the longitudinal axis of the Zn_2GeO_4 nanowires follows [110] or [001] as preferred directions, determined by TEM /STEM imaging analysis. In the latter case, Zn_2GeO_4 NWs with [001] orientation serve as substrate for the growth of SnO_2 crystals where the a-GeO_2 particles act as nucleation sites, leading to a skewer-like shape. The [001] orientation of the central Zn_2GeO_4 NWs exposes lateral surfaces that have good lattice match with the rutile phase of SnO_2. On the other hand, a rather high amount of Ge is found into the SnO_2 particles, which could even lead to the stabilization of small clusters of a solid solution of both oxides

(GeO_2 and SnO_2). However, the structural analysis confirms the rutile symmetry. Once the radial growth of the SnO_2 reaches a critical size, the growth may continue further parallel to the nanowire axis, if there is still tin available in the source materials, tending to close the gaps between adjacent crystals. The luminescence bands of this heavily Ge-doped SnO_2 obtained by cathodoluminescence in the SEM and photoluminescence are similar to those reported in SnO_2. CL and PL experiments have also revealed that some SK structures display light confinement effects, such as the presence of optical resonances in the luminescence spectra. The analysis demonstrates that Fabry-Perot resonances occur due to reflection at the SnO_2 end-facets of light propagating parallel to the NWs. These results show that SK structures may act as an array of optical microcavities sustained by a nanowire, with potential applications in UV-blue optoelectronic devices.

Acknowledgement

This work was supported by the Spanish Ministry of Innovation, Science and Technology through Research Projects MAT-2015-65274-R/FEDER, RTI2018-097195-B-I00 and M-ERA.NET PCIN-2017-106.

Supporting Information Available

- Complementary SEM and TEM characterization of the NW heterostructures.

References

(1) Guan, X.; Becdelievre, J.; Meunier, B.; Benali, A.; Saint-Girons, G.; Bachelet, R.; Regreny, P.; Botella, C.; Grenet, G.; Blanchard, N., et al. GaAs core/$SrTiO_3$ shell nanowires grown by molecular beam epitaxy. *Nano letters* **2016**, *16*, 2393–2399.

(2) Borgström, M. T.; Zwiller, V.; Müller, E.; Imamoglu, A. Optically bright quantum dots in single nanowires. *Nano letters* **2005**, *5*, 1439–1443.

(3) Tatebayashi, J.; Kako, S.; Ho, J.; Ota, Y.; Iwamoto, S.; Arakawa, Y. Room-temperature lasing in a single nanowire with quantum dots. *Nature Photonics* **2015**, *9*, 501.

(4) Gazibegovic, S. et al. Epitaxy of advanced nanowire quantum devices. *Nature* **2017**, *548*, 434–438.

(5) Mizoguchi, H.; Kamiya, T.; Matsuishi, S.; Hosono, H. A germanate transparent conductive oxide. *Nature communications* **2011**, *2*, 470.

(6) Pearton, S.; Yang, J.; Cary IV, P. H.; Ren, F.; Kim, J.; Tadjer, M. J.; Mastro, M. A. A review of Ga_2O_3 materials, processing, and devices. *Applied Physics Reviews* **2018**, *5*, 011301.

(7) Heiss, M.; Fontana, Y.; Gustafsson, A.; Wüst, G.; Magen, C.; O'regan, D.; Luo, J.; Ketterer, B.; Conesa-Boj, S.; Kuhlmann, A., et al. Self-assembled quantum dots in a nanowire system for quantum photonics. *Nature materials* **2013**, *12*, 439.

(8) Kuchibhatla, S. V.; Karakoti, A.; Bera, D.; Seal, S. One dimensional nanostructured materials. *Progress in materials science* **2007**, *52*, 699–913.

(9) Alonso-Orts, M.; Sánchez, A. M.; Hindmarsh, S. A.; López, I.; Nogales, E.; Piqueras, J.; Méndez, B. Shape engineering driven by selective growth of SnO_2 on doped Ga_2O_3 nanowires. *Nano Letters* **2017**, *17*, 515–522.

(10) Day, R. W.; Mankin, M. N.; Gao, R.; No, Y.-S.; Kim, S.-K.; Bell, D. C.; Park, H.-G.; Lieber, C. M. Plateau–Rayleigh crystal growth of periodic shells on one-dimensional substrates. *Nature nanotechnology* **2015**, *10*, 345.

(11) Tian, W.; Lu, H.; Li, L. Nanoscale ultraviolet photodetectors based on onedimensional metal oxide nanostructures. *Nano Research* **2015**, *8*, 382–405.

(12) Zhou, X.; Zhang, Q.; Gan, L.; Li, X.; Li, H.; Zhang, Y.; Golberg, D.; Zhai, T. High—Performance Solar-Blind Deep Ultraviolet Photodetector Based on Individual Single-Crystalline Zn_2GeO_4 Nanowire. *Advanced Functional Materials* **2016**, *26*, 704–712.

(13) Liu, Z.; Liang, B.; Chen, G.; Yu, G.; Xie, Z.; Gao, L.; Chen, D.; Shen, G. Contact printing of horizontally aligned Zn_2GeO_4 and $In_2Ge_2O_7$ nanowire arrays for multi-channel field-effect transistors and their photoresponse performances. *Journal of Materials Chemistry C* **2013**, *1*, 131–137.

(14) He, H.; Zhang, Y.; Pan, Q.; Wu, G.; Dong, G.; Qiu, J. Controllable synthesis of Zn_2GeO_4:Eu nanocrystals with multi-color emission for white light-emitting diodes. *J. Mater. Chem. C* **2015**, *3*, 5419–5429.

(15) Tien, L.-C.; Yang, F.-M.; Huang, S.-C.; Fan, Z.-X.; Chen, R.-S. Single Zn_2GeO_4 nanowire high-performance broadband photodetector. *Journal of Applied Physics* **2018**, *124*, 174503.

(16) Wang, J.; Yan, C.; Magdassi, S.; Lee, P. S. Zn_2GeO_4 Nanowires As Efficient Electron Injection Material for Electroluminescent Devices. *ACS Applied Materials & Interfaces* **2013**, *5*, 6793–6796, PMID: 23838396.

(17) Yi, R.; Feng, J.; Lv, D.; Gordin, M. L.; Chen, S.; Choi, D.; Wang, D. Amorphous Zn2GeO4 nanoparticles as anodes with high reversible capacity and long cycling life for Li-ion batteries. *Nano Energy* **2013**, *2*, 498 – 504.

(18) Stevens, R.; Woodfield, B. F.; Boerio-Goates, J.; Crawford, M. K. Heat capacities, third-law entropies and thermodynamic functions of the negative thermal expansion material Zn_2GeO_4 from T=(0 to 400) K. *The Journal of Chemical Thermodynamics* **2004**, *36*, 349–357.

(19) Hidalgo, P.; López, A.; Méndez, B.; Piqueras, J. Synthesis and optical properties of Zn_2GeO_4 microrods. *Acta Materialia* **2016**, *104*, 84–90.

(20) López, I.; Nogales, E.; Méndez, B.; Piqueras, J.; Peche, A.; Ramírez-Castellanos, J.; González-Calbet, J. M. Influence of Sn and Cr doping on morphology and luminescence of thermally grown Ga_2O_3 nanowires. *The Journal of Physical Chemistry C* **2013**, *117*, 3036–3045.

(21) Hidalgo, P.; Méndez, B.; Piqueras, J. Sn doped GeO_2 nanowires with waveguiding behavior. *Nanotechnology* **2008**, *19*, 455705.

(22) Zheng, T.; Li, Z.; Chen, J.; Shen, K.; Sun, K. Transitions of microstructure and photoluminescence properties of the Ge/ZnO multilayer films in certain annealing temperature region. *Applied surface science* **2006**, *252*, 8482–8486.

(23) Yu, Y.; Kim, G.; Min, B.; Kim, S. Optical characteristics of Ge doped ZnO compound. *Journal of the European Ceramic Society* **2004**, *24*, 1865–1868.

(24) Gu, Z.; Liu, F.; Li, X.; Pan, Z. W. Luminescent GeO_2–Zn_2GeO_4 hybrid one dimensional nanostructures. *CrystEngComm* **2013**, *15*, 2904–2908.

(25) Day, R. W.; Mankin, M. N.; Lieber, C. M. Plateau–Rayleigh crystal growth of nanowire heterostructures: strain-modified surface chemistry and morphological control in one, two, and three dimensions. *Nano letters* **2016**, *16*, 2830–2836.

(26) Bechelany, M.; Riesterer, J. L.; Brioude, A.; Cornu, D.; Miele, P. Rayleigh instability induced SiC/SiO_2 necklace like nanostructures. *CrystEngComm* **2012**, *14*, 7744–7748.

(27) Kumar, A.; Kundu, S.; Samantaray, D.; Kundu, P.; Zanaga, D.; Bals, S.; Ravishankar, N. Designing diameter-modulated heterostructure nanowires of PbTe/Te by controlled dewetting. *Nano letters* **2017**, *17*, 7226–7233.

(28) Mead-Hunter, R.; King, A. J.; Mullins, B. J. Plateau Rayleigh instability simulation. *Langmuir* **2012**, *28*, 6731–6735.

(29) Chu, Y.; Jing, S.; Yu, X.; Zhao, Y. High-Temperature Plateau–Rayleigh Growth of Beaded SiC/SiO_2 Nanochain Heterostructures. *Crystal Growth & Design* **2018**, *18*, 2941–2947.

(30) Zeng, Z.; Li, Y.; Chen, J.; Zhou, W. GaP/GaO_x Core- Shell Nanowires and Nanochains and Their Transport Properties. *The Journal of Physical Chemistry C* **2008**, *112*, 18588–18591.

(31) Kolb, F.; Hofmeister, H.; Zacharias, M.; Gösele, U. On the morphological instability of silicon/silicon dioxide nanowires. *Applied Physics A* **2005**, *80*, 1405–1408.

(32) Watanabe, A.; Kikuchi, T.; Tsutsumi, M.; Takenouchi, S.; Uchida, K. Solid solubility of GeO_2 in SnO_2. *Journal of the American Ceramic Society* **1983**, *66*, c104–c105.

(33) Sharma, A.; Kim, D.; Yoo, S.-I. Subsolidus phase diagram in the GeO_2–ZnO–SnO_2 system at 1100 °C in air. *Ceramics International* **2018**, *44*, 9848–9853.

(34) Kavanagh, K. L. Misfit dislocations in nanowire heterostructures. *Semiconductor Science and Technology* **2010**, *25*, 024006.

(35) Liu, Z.; Jing, X.; Wang, L. Luminescence of native defects in Zn_2GeO_4. *Journal of The Electrochemical Society* **2007**, *154*, H500–H506.

(36) Kim, H. W.; Na, H. G.; Yang, J. C.; Lee, C. Temperature-controlled synthesis of Zn_2GeO_4 nanowires in a vapor–liquid–solid mode and their photoluminescence properties. *Chemical engineering journal* **2011**, *171*, 1439–1445.

(37) Dolado, J.; Hidalgo, P.; Méndez, B. Correlative study of vibrational and luminescence properties of Zn_2GeO_4 microrods. *physica status solidi (a)* **2018**, *215*, 1800270.

(38) Maestre, D.; Cremades, A.; Piqueras, J. Cathodoluminescence of defects in sintered tin oxide. *Journal of applied physics* **2004**, *95*, 3027–3030.

(39) Maestre, D.; Cremades, A.; Piqueras, J. Growth and luminescence properties of micro- and nanotubes in sintered tin oxide. *Journal of applied physics* **2005**, *97*, 044316.

(40) Rigby, O. M.; Stamp, A. V.; Hindmarsh, S. A.; Alonso-Orts, M.; Nogales, E.; Méndez, B.; Sanchez, A. M. Direct observation of tunnelled intergrowth in SnO_2/Ga_2O_3 complex nanowires. *Nanotechnology* **2018**, *30*, 054004.

(41) García-Tecedor, M.; Maestre, D.; Cremades, A.; Piqueras, J. Tailoring optical resonant cavity modes in SnO_2 microstructures through doping and shape engineering. *Journal of Physics D: Applied Physics* **2017**, *50*, 415104.

(42) Jin, C.; Kim, H.; Ryu, H.-Y.; Kim, H. W.; Lee, C. Subwavelength Optical Resonant Cavity-Induced Enhancement of the Near-Band-Edge Emission from ZnO-Core/SnO_2-Shell Nanorods. *The Journal of Physical Chemistry C* **2011**, *115*, 8513–8518.

(43) Atay, F.; Bilgin, V.; Akyuz, I.; Ketenci, E.; Kose, S. Optical characterization of SnO_2:F films by spectroscopic ellipsometry. *Journal of Non-Crystalline Solids* **2010**, *356*, 2192 – 2197.

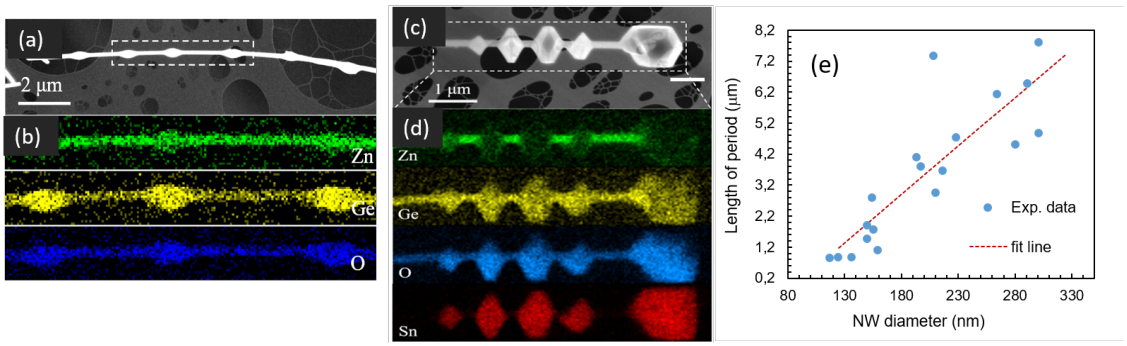

Figure 1: Representative SEM images and EDS maps of a NL-like structure (a)-(b) and of a skewer-like (SK) structure (c)-(d). The white dashed box in SEM images indicates the area where the EDS maps were taken, showing the elemental distribution of Zn (green), Ge (yellow), O (blue) and Sn (red) elements. (e) For NLs, plot of the length of the period of the beads as a function of the NW diameter taken from a representative number of NLs from T-5. The linear dependence supports the P-R mechanism for the NL formation.

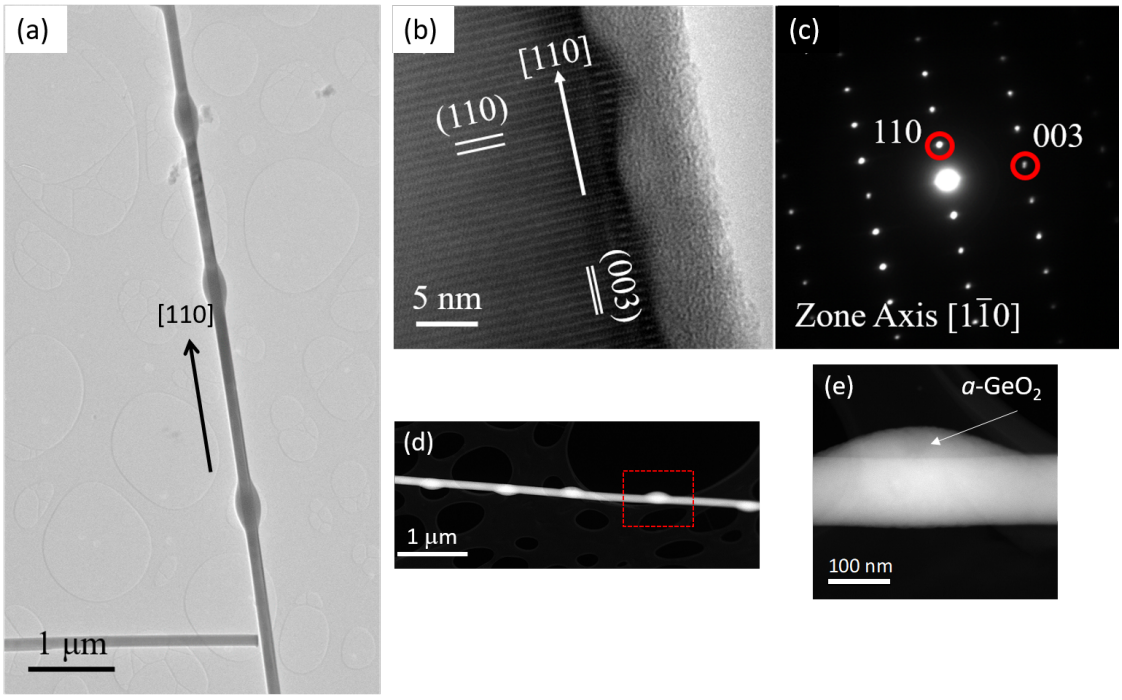

Figure 2: (a) Low-magnification TEM image of a necklace-like (NL) Zn_2GeO_4/GeO_2 structure. (b) HRTEM image and (c) SAED pattern taken from the Zn_2GeO_4 NL in (a). (b) and (c) were recorded along the [1$\bar{1}$0] zone axis and demonstrating a [110] growth direction for the NW. (d)-(e) ADF-STEM images of a NL and the detail of the red-squared amorphous bead in (d) formed on one side of the NW.

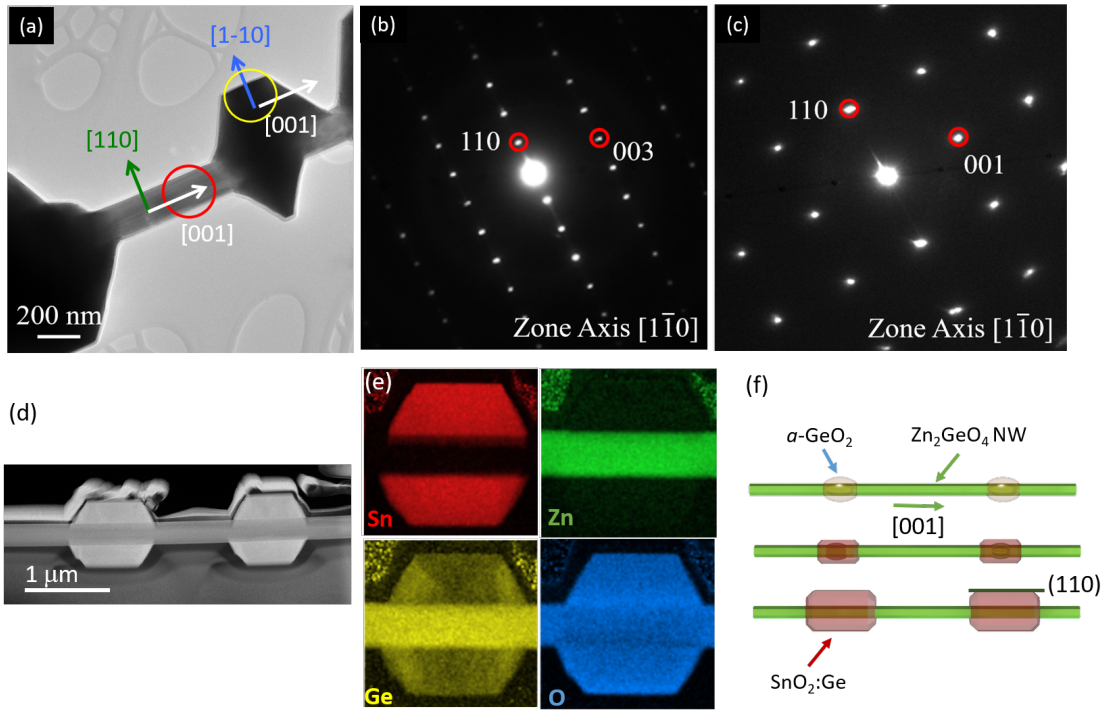

Figure 3: (a) TEM image of the wire from a skewer-like structure. (b) HRTEM image and (c) SAED pattern taken from the red circled region in (a), corresponding to the [1$\bar{1}$0] zone axis of the Zn_2GeO_4 lattice. (d) ADF image of a cross-section parallel the axis wire of one of the SK structures. (e) Sn, Zn, Ge and O mapping of one of the SnO_2 crystals. (f) Sketch illustrating the growth model.

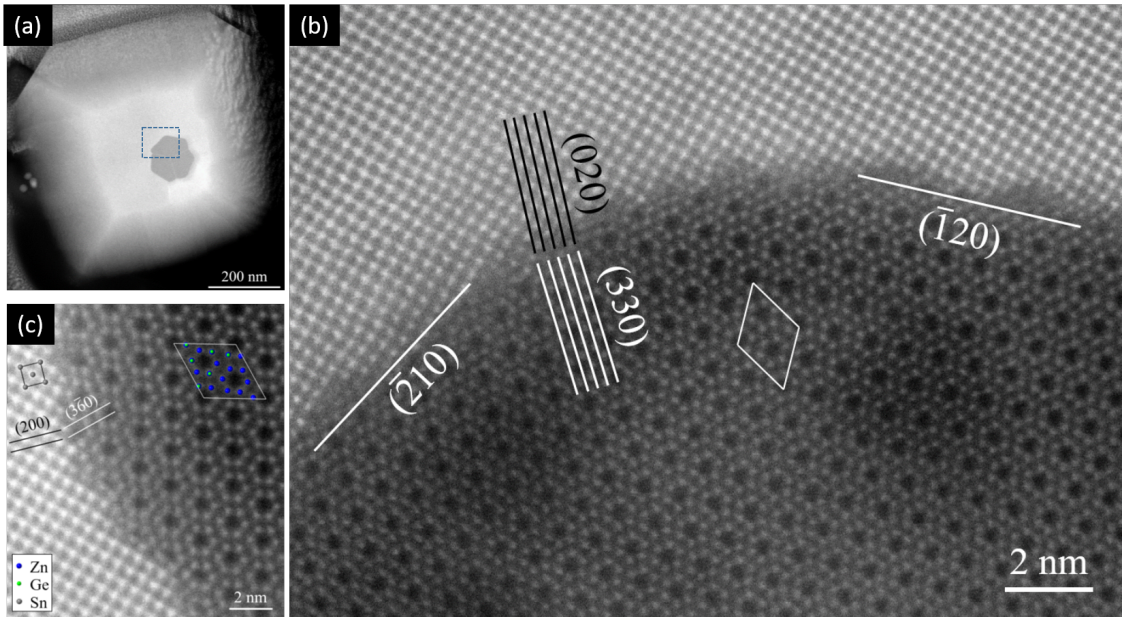

Figure 4: (a) ADF-STEM image of the cross section perpendicular to the NW axis as a whole. (b) Atomic resolution ADF image of the NW-particle interface from (a). The $(\bar{2}10)$ and $(\bar{1}20)$ surface facets for the Zn_2GeO_4 nanowire have been marked, as well as the (330) planes for Zn_2GeO_4 and the (020) planes for SnO_2. A unit cell of Zn_2GeO_4 is shown for reference. (c) Detail of the NW-particle interface showing the alignment of $(3\bar{6}0)$ Zn_2GeO_4 and (200) planes SnO_2. Cation positions of Zn, Ge, and Sn are colored blue, green and purple, respectively.

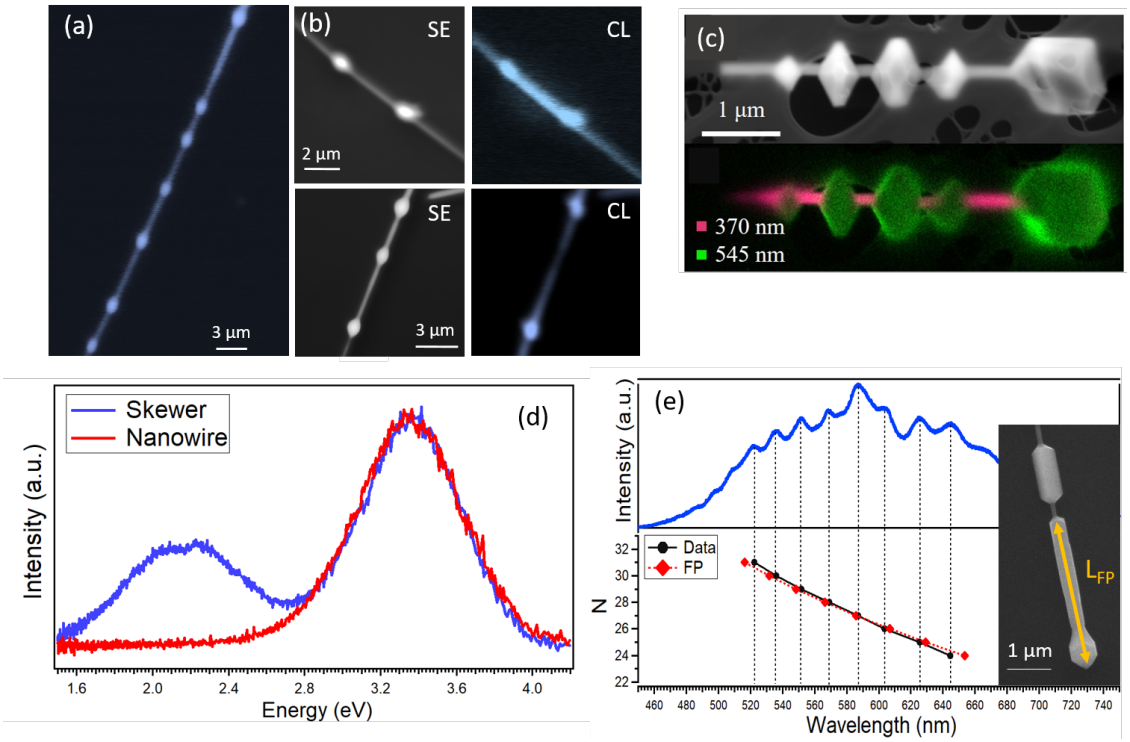

Figure 5: (a) CL image of a necklace structure. (b) SE and CL images of NLs with particular CL enhancement between beads (top) or quenching (bottom). (c) SE and monochromatic CL mapping at 370 nm and 545 nm of a SK structure. (d) Local CL spectra from the central Zn_2GeO_4 NW (red line) and the SnO_2 particle (blue line). (e) Top: PL spectrum recorded from the SnO_2 crystal, shown in the SE image. Bottom: wavelength maxima are fitted with Fabry-Perot resonances (black dots) and compared with theoretical calculations (red diamonds). The calculated L_{FP} value agree with the length of the SnO_2 measured in the SEM.

Graphical TOC Entry

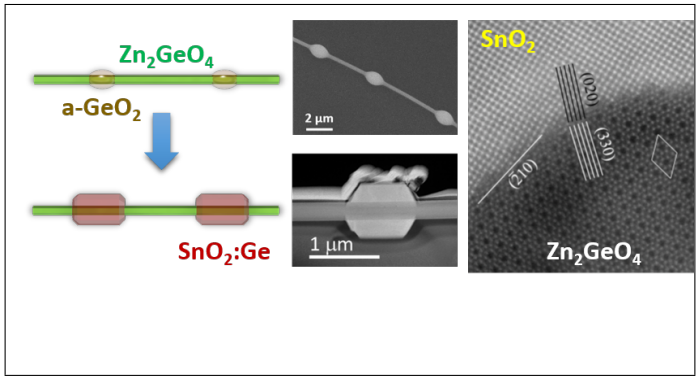

For Table of Contents Use Only

Zn_2GeO_4/SnO_2 nanowire heterostructures driven by Plateau-Rayleigh instability

Jaime Dolado, Kate L Renforth, James E Nunn, Steve A. Hindsmarsh, Pedro Hidalgo, Ana M Sánchez, Bianchi Méndez

Synopsis

Herein we present results on heterostructures formed by Zn_2GeO_4 nanowires, which sustain evenly distributed SnO_2 particles. The Plateau-Rayleigh instability produces a sequence of amorphous germanium oxide beads along the nanowire that act as nucleation sites for SnO_2 particles along the NW mimicking their pattern. A potential application as an array of optical micro-cavities is envisaged.